INTERNATIONAL JOURNAL OF AUTOMOTIVE AND MECHANICAL ENGINEERING
ISSN: 2229-8649 e-ISSN: 2180-1606
VOLUME 22, ISSUE 2, 2025, 12316 - 12331
DOI: https://doi.org/10.15282/ijame.22.2.2025.6.0943

RESEARCH ARTICLE

Experimental Investigation and Optimization of Process Parameters on Abrasive Water Jet Machining of Inconel X-750 Superalloy

Vikas Sisodia[1], Dharmalingam Ganesan[2*], Arun Prasad Murli[3], Mithali Mane[4], Sachin Salunkhe[5,6], Shailendra Kumar[7]

[1]Department of Automation and Robotics Engineering, Prestige Institute of Engineering Management and Research, Indore, M.P, India
[2,3]Department of Mechanical Engineering, Vel Tech Rangarajan Dr. Sagunthala R&D Institute of Science and Technology, Avadi, Chennai, India
[4]Department of Manufacturing Engineering and Industrial Management, COEP Technological University, Pune, Maharashtra, India
[5]Department of Biosciences, Saveetha School of Engineering, Saveetha Institute of Medical and Technical Sciences, Chennai, T.N., India
[6]Gazi University Faculty of Engineering, Department of Mechanical Engineering, Maltepe, Ankara, Turkey
[7]Department of Mechanical Engineering, Sardar Vallabhbhai National Institute of Technology Surat, Gujarat, India

ABSTRACT – Inconel X-750 is a nickel chromium-based superalloy with various industrial applications due to its exceptional mechanical properties. It is used in aerospace applications, gas turbine rotor components, nuclear power plant parts, etc. Inconel X-750 has a machinability index ranging from 12 to 16, which makes it hard to cut material using traditional machining processes. Therefore, there is a need to find a modern alternative to machine the Inconel X-750 superalloy. Many industries employ well-established Abrasive Waterjet Machining (AWJM) technology to cut different types of materials. However, the applicability of AWJM of Inconel X750 is not available in the scientific domain. Therefore, the objective finalized for the present study is to conduct thorough experimental research and process parameter optimization in the domain AWJM of Inconel X-750. To accomplish the above objective, the impact of process variables, such as water pressure (WP), standoff distance (SOD), and nozzle traverse speed (TS) on important performance indicators, namely material removal rate (MRR), kerf properties and surface roughness (R_a) of machined components. Central composite design (CCD), a Response Surface Methodology (RSM), was used to design the experimental trials in this study. After conducting the experimental trials, the results obtained were assessed for the statistical relevance of the process factors to response characteristics. For this, the well-known statistical approach, i.e., Analysis of Variance (ANOVA), is employed. The findings of the present work suggested that traverse speed is a highly influential factor on Inconel X-750's MRR as well as R_a. The analysis also reveals that TS and WP are key factors influencing the kerf characteristics of the workpiece. To facilitate precise predictions of material performance under the influence of process variables, a regression model has been developed, allowing the prediction of response within the design space. The developed model serves well for optimizing machining conditions, thereby improving the performance of the process. The values predicted for the responses by the model are in good agreement with experimentally obtained response values with permissible error. Post-optimizing the process performance, the optimized process parameters were found to be WP of 380 MPa, TS of 38.6 mm/min, and SOD of 2 mm, which produced a R_a of 4.1μm, the kerf taper angle of 0.4 degrees, and MRR of 907 mm^3/min. The optimized parameters yielded satisfactory results.

ARTICLE HISTORY

Received	:	06th Dec. 2024
Revised	:	10th Apr. 2025
Accepted	:	03rd May 2025
Published	:	01st June 2025

KEYWORDS
Inconel X-750
Heat resisting alloy
AWJM
Process parameters
Kerf taper
Surface roughness

1. INTRODUCTION

Superalloys belong to group VIII elements (nickel, cobalt, or iron, with nickel as the maximum share), to which a certain quantity of alloying elements are added. This material retains an exceptional mechanical performance with good surface integrity at elevated temperatures [1]. Here, the Inconel X-750 material is a precipitation hardenable nickel-chromium alloy renowned for its excellent high strength, oxidation resistance, and capability to withstand corrosion at temperatures as high as 700°C. Its exceptional stability at cryogenic temperatures makes high-performance applications in harsh environments possible. The Inconel X-750 has an extensive variety of industrial applicability, mainly in large pressure vessels, thrust chambers of the engines of rockets, thrust reversers, heat-resistant structural material in nuclear power plants, ducting systems of hot air, heat treating fixtures, test machine grips, forming tools, and extrusion process die thus and so on [2].In gas turbine applications, the Inconel X-750 is widely used for critical structural components such as turbine rotor blades, wheels, and bolts. It can give a desirable performance, such as in withstanding extreme temperatures and mechanical stress under demanding operational conditions. For miscellaneous application domains such as aerospace, the Inconel X-750 material is employed for various components, including airframes, thrust reversers, hot-air ducting structures, and allied systems. Its high-temperature resistance and mechanical strength make it well-suited for

***CORRESPONDING AUTHOR | D. Ganesan** | ✉ gdharmalingam@veltech.edu.in

environments that demand durability and thermal stability. It is also thus used to fabricate springs and fasteners, which can be used in temperatures much below zero degrees centigrade to 650°C [3]. The Superalloy X-750 Inconel alloy's strong toughness and low thermal conductivity make it challenging to machine conventionally because of the heat generated at the workpiece-tool interface. This leads to low surface polish, extremely low production rates, and a high tool wear rate. Although they yield exceptional surface finishes at high speeds, polycrystalline boron nitride (PCBN) cutting tools and cubic boron nitride (CBN) cutting tools have a notably high machining cost [4]. Inconel X-750, a heat-resistant superalloy, is thus one of the hardest nickel-based alloys. Hence, its machinability index is in the range of 12 to 16, which is very low and makes it one of the hardest-to-machine materials with traditional machining processes.

Thus, there is a need to find a modern alternative to machine the Inconel X-750 superalloy. The abrasive water jet machining (AWJM) process is a well-established process and is widely used in industries to machine various materials. There is the non-existence of a heat-affected zone (HAZ) and residual stress post-machining operation. Also, it facilitates rapid work setup and does not require a tool change. Due to this, the machining cost is lower. The process mechanics involved in the AWJM process make it possible to easily machine difficult-to-cut materials in less time. In this process, when a highly pressurized abrasive waterjet is made to pass through a small opening of a converging nozzle, it acquires very high momentum. Simultaneously, in the nozzle, the abrasives are mixed with this water jet, and slowly, this mixture accelerates, resulting in a high-speed abrasive water jet. Material removal occurs from the workpiece by the impact of an abrasive waterjet, creating material erosion upon their interaction [5]. Using this process, various materials, from hard materials like ceramics to soft materials like mild steel and aluminum, can be easily machined. As high-speed abrasive waterjets are involved, almost no heat or negligible heat is generated during machining. So, no heat-affected zones (HAZ) exist, and residual stress is also observed [6]. Also, characteristics such as very low cutting forces, improved material removal rate, good precision, and high accuracy have made this process popular in industries. The R_a of the machined surface and kerf taper properties are essential quality measures in this machining method.

Worldwide, researchers have continuously contributed to improving the cutting characteristics and performance of AWJM superalloys. For example, Geethapriyan et al. [5] investigated the impact of process factors of AWJM on material removal rate (MRR) and surface characteristics of the Inconel 600 superalloy with two abrasive grain sizes. Reddy et al. [7] presented an investigation on the optimization of process factors to maximize and improve MRR and decrease the R_a of the Inconel 800H. Satyanarayana and Shrikar [8] also performed an experimental study on minimizing kerf properties and maximizing MRR in AWJM of Inconel-718 superalloy. It was reported that water pressure impacts MRR and kerf width more than other remaining parameters. Kishore and Raju [9] selected a set of optimized parameters of AWJM to machine the Inconel-625 superalloy. They investigated the impact of process variables, namely TS, WP and SOD on MRR and surface roughness (SR). Fowler et al. [10] studied the impact of TS, abrasive size, and number of passes on the waviness of the titanium alloy Ti-6Al-4V. It was found that at higher traverse rates, less surface roughness is observed, but waviness increases due to the less abrasive passes by the designated area. Mogul et al. [11] analyzed the influence of process factors, namely nozzle diameter, nozzle TS, the mass flux of abrasives, and water pressure, on the depth of cut in AWJM of Titanium alloy (Ti-6Al-4V). Researchers reported that process parameters directly impact jets' penetration depth. Pal and Chaudhari [12] investigated the impact of process factors such as SOD, water pressure, and abrasive particle size on the depth of cut, MRR, and surface roughness in blind pocket machining of the titanium alloy. It was concluded that at higher water pressure, more penetration depth, i.e., more depth cut, can be achieved along with high MRR. However, the surface finish is more at the corners than on the walls. By decreasing the abrasive size, a good surface finish was obtained. Vasanth et al. [13] assessed the influence of key process parameters, specifically abrasive mass flow rate (AMFR) and SOD, on MRR and SR during AWJM of the Ti-6Al-4V. Their findings reveal that by increasing the abrasive particles mass flow rate and SOD surface waviness and roughness increased. So, there must have been a trade-off between material removal efficiency and surface quality. Alberdi et al. [14] conducted a study that explored the impact of various process parameters such as nozzle diameter, TS, AMFR, and WP on the SR achieved while machining Ti-6Al-4V and carbon fiber-reinforced polymer (CFRP) by AWJM. The findings of the work show a peculiar feature. The positive kerf taper was observed in Ti-6Al-4V, while CFRP exhibited a negative kerf taper. Additionally, it was reported that surface roughness could be minimized to approximately 6.5 µm at higher nozzle traverse speeds, suggesting that optimal speed is critical in improving the surface finish.

Olsen and Zeng [15] made comparisons between three non-traditional machining techniques. AWJM, electric-discharge machining process (EDM), and laser beam machining process (LBM) are used to process carbides and Inconel super alloys to achieve cut-on maximum thickness and MRR. The findings of this work highlighted that AWJM outperforms laser cutting while working with thicker materials due to its ability to penetrate greater depths. Additionally, the AWJM demonstrated a higher MRR than EDM, making it a more desirable process for applications requiring faster material removal. These results emphasize the advantages of AWJM in scenarios demanding high efficiency and the ability to cut thick, tough materials. Reddy et al. [16] examined the impact of various process parameters on the MRR, SR, and kerf characteristics while machining Inconel 625 with AWJM. It was observed that TS and AMFR significantly influenced MRR and surface finish. However, while evaluating kerf properties, standoff distance and the above two process parameters emerged as critical process factors. Vasudevan et al. [17] examined the impact of WP, AFR, and SOD on the performance and quality of abrasive waterjet drilling applied to Yttrium-Stabilized Zirconia (YSZ) coated Inconel 718. Among the parameters examined, the AFR and SOD were identified as the most influential factors affecting both the efficiency and precision of the drilling process. The results highlighted the importance of optimizing the process parameters to enhance machining quality and operational efficiency when working with advanced coatings and superalloy substrates. Trivedi et al. [18] investigated the influence of process parameters, such as namely the WP, TS, and SOD, on SR in AWJM of austenitic stainless steel (AISI 316L). They observed that nozzle TS is the most significant process factor impacting the roughness of the surface. Also, increasing WP gives a good surface finish, but at a higher value of SOD, TS creates more striation marks. Sisodia et al. [20] studied the influence of nozzle TR, standoff height, and WP on the surface and kerf properties of SS 440C (AISI). They reported that surface finish improved by increasing the WP and by decreasing standoff height and nozzle traverse rate. Qian et al. [29] investigated the effect of abrasive waterjet (AWJ) machining variables on the surface integrity of AA7075 aluminum alloy when subjected to circular cutting paths. The research reveals that while both straight and round cuts share similar material removal mechanisms, circular cuts result in inferior surface quality, particularly as the radius of curvature decreases.

Notably, the surface roughness at the bottom of the workpiece with a circular cut radius of 2.5 mm was found to be more than twice that of a linear cut. The study identifies tangential velocity as one of the most significant process variables affecting roughness, followed by the radius of the circular cut, working pressure, and standoff distance. To optimize cutting quality in circular AWJ machining, the authors recommend prioritizing the adjustment of tangential velocity. Chandra Shekar et al. [30] investigated the application of abrasive waterjet (AWJ) machining as a surface engineering solution for repairing aerospace composite components fabricated through additive manufacturing (AM). Recognizing the limitations of traditional thermal-based machining methods, the study highlights AWJ's non-thermal precision in enhancing surface topography, also improving adhesion, and minimizing structural defects such as delamination and fiber pull-out. Through systematic variation of AWJ process parameters, the researchers demonstrate how optimized machining can yield superior surface finishes and facilitate high-integrity bonding in repair scenarios. This work signifies the growing domain of literature advocating for AWJ as a robust, efficient, and damage-free technique in the context of composite repair strategies within the aerospace sector. Felhő et al. [31] studied the relationship between two-dimensional (2D) and three-dimensional (3D) surface roughness measurements on AlMgSi0.5 aluminum alloy subjected to abrasive waterjet (AWJ) cutting. The research reveals that AWJ machining typically produces anisotropic surface textures, with roughness increasing from the jet's entry to exit points. Notably, 3D areal roughness parameters (S_a and S_z) consistently exhibit higher values than their 2D profile counterparts (P_a and P_z), especially at elevated feed speeds.

The study emphasizes that 3D measurements offer a more comprehensive representation of surface topography, capturing variations that 2D assessments might overlook. Consequently, for accurate characterization of AWJ-machined surfaces, particularly those with anisotropic features, the use of 3D roughness parameters is suggested over traditional 2D metrics. Karkalos et al. [32] have shown the application of statistical probability distributions to model surface roughness profiles resulting from abrasive waterjet (AWJ) milling processes. Recognizing the limitations of conventional models that are primarily focused on basic roughness parameters like R_a and R_z, the authors propose a more comprehensive approach by incorporating additional pointers such as skewness (R_{sk}), kurtosis (R_{ku}), and the R_p/R_v ratio. Through a three-stage evaluation of six different probability distributions, the study identifies the Weibull distribution as particularly effective in approximating these multiple roughness parameters with sufficient accuracy. This approach offers a practical and cost-effective method for predicting surface morphologies and enhancing the ability to optimize surface quality in AWJ-milled components without using complex statistical tools or specialized software.

The above literature review reveals that worldwide researchers are progressively exploring non-traditional and cost-effective machining methods for processing Superalloys such as the Inconel X750. Their research efforts primarily focus on enhancing the quality of machining operations by investigating how well process parameters influence key outcomes, such as surface roughness, kerf characteristics, and the MRR. However, studies specifically addressing the AWJM of Inconel x750 superalloys are not available, particularly regarding the impact of process variables on surface finish, MRR, and kerf taper. Notably, a lack of research focused on Inconel X-750, a material with a machinability index between 12 and 16 (which is very low), indicates significant challenges with traditional machining processes and techniques. A low machinability index suggests that the material is less machinable. Therefore, very specialized tooling solutions are required to machine the Inconel X-750, increasing the machining cost significantly. Given these challenges, it is essential to explore modern machining alternatives to process superalloys like Inconel X-750 effectively. To address this research gap, the Abrasive Waterjet Machining Process, one of the nontraditional machining techniques, is considered in the present study. A detailed experimental analysis is undertaken to study and assess the influence of three critical process parameters in WP, TS, and SOD on SR, MRR, and kerf taper by using the AWJM technique. The objective is to identify optimal machining conditions for improving performance and efficiency with this difficult-to-machine superalloy. The methodology and flow of research work drafted to accomplish the above-mentioned goals and objectives are hereby depicted in Figure 1.

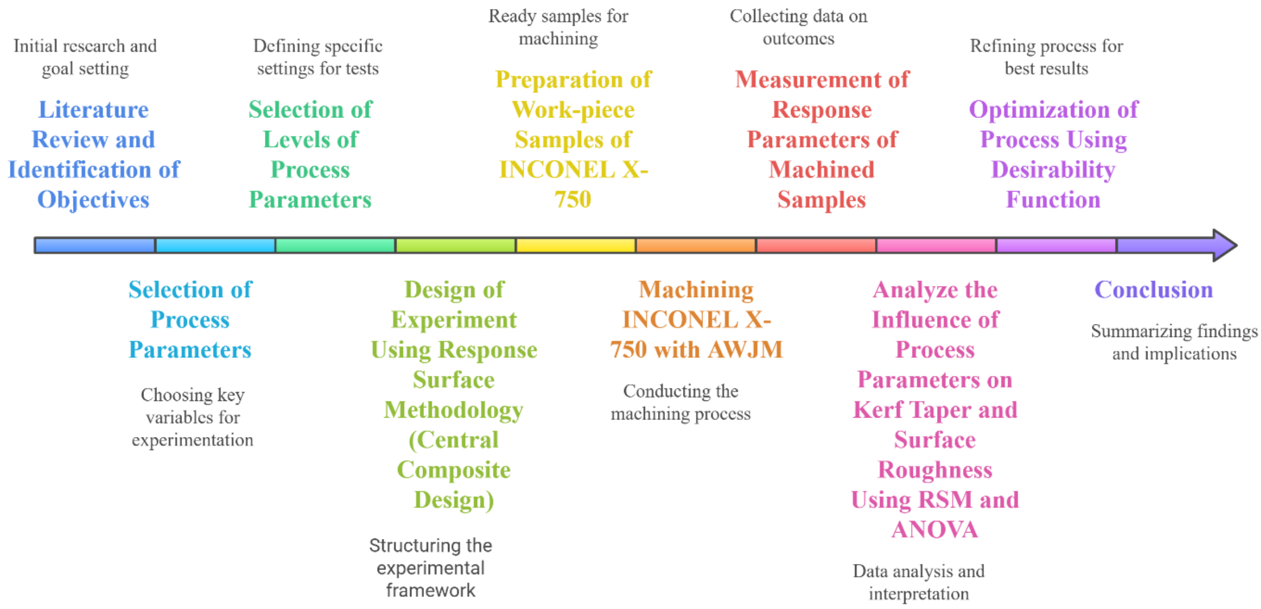

Figure 1. The methodology adopted in the present work

2. MATERIALS AND METHODS

For the current research, the experimental design was structured using the CCD within the framework of RSM after analyzing the process variables. The CCD is one of the feasible designs of experiment (DoE) approach used in experimental trials, as it needs fewer design points but can give sufficient output statistics to assess the lack of fit. Based on the CCD DoE, 20 experimental trial runs are proposed. For the current investigation, these 20 experiments can be bifurcated into six centered runs, six axial runs, and eight factorial runs. But, if the comparisons are made with the full factorial design for three factors and, let's say, at four levels, then, according to the full factorial design, the total number of trials obtained is 64. Although all possible arrangements of process factors are taken into account in the full factorial design of experiments, performing 64 of these experiments is utterly difficult. Unlike traditional trial-and-error or one-factor-at-a-time methods, CCD-RSM enables the development of a second-degree polynomial equation model, which captures linear and quadratic effects and interactions between factors. This makes it particularly suitable for scenarios where the relationship between process parameters and response variables is non-linear. While compared to heuristic or machine learning approaches such as Genetic Algorithms (GA) or Artificial Neural Networks (ANN), CCD-RSM offers a more interpretable and statistically validated modeling framework. It provides powerful tools such as ANOVA, response surface plots, and desirability functions, thus facilitating deeper insights into process behavior and variable sensitivity.

Additionally, unlike Taguchi methods, which primarily focus on robustness and signal-to-noise analysis with limited interaction modeling, the CCD-RSM provides a more comprehensive representation of the response surface, making it a preferred choice for fine-tuning process parameters to reach global optima. Therefore, CCD-RSM was relatively more suitable for achieving reliable prediction, robust optimization, and enhanced process understanding in the context of this research. Also, the amount of material required (Inconel X-750, an expensive superalloy) and the processing of experimental information are more critical in such cases, along with the high research and experiment costs. As sufficient and relevant information from 20 trials can be obtained from the CCD, CCD has been selected for the current investigation. The machining of the Inconel X-750 superalloy is performed on a computer-controlled flying arm AWJM setup (Make- MIS Innovative International Ltd., Ahmedabad, India), as shown in Figure 2. Water pressure is set by using a dial indicator of the pumping system. SOD is carefully and accurately set using slip gauges, and traverse speed is varied through computer control. The nozzle diameter, the diameter of the orifice, and the impingement angle are held constant at 0.76 mm, 0.3 mm, and 90 degrees, respectively. The garnet abrasive mass flow rate is kept at 380 g/min. After that, the analysis of the results obtained is performed by using ANOVA. A regression model is fitted to estimate the values of R_a and kerf taper properties for different combinations. Optimization of process parameters is carried out to minimize responses.

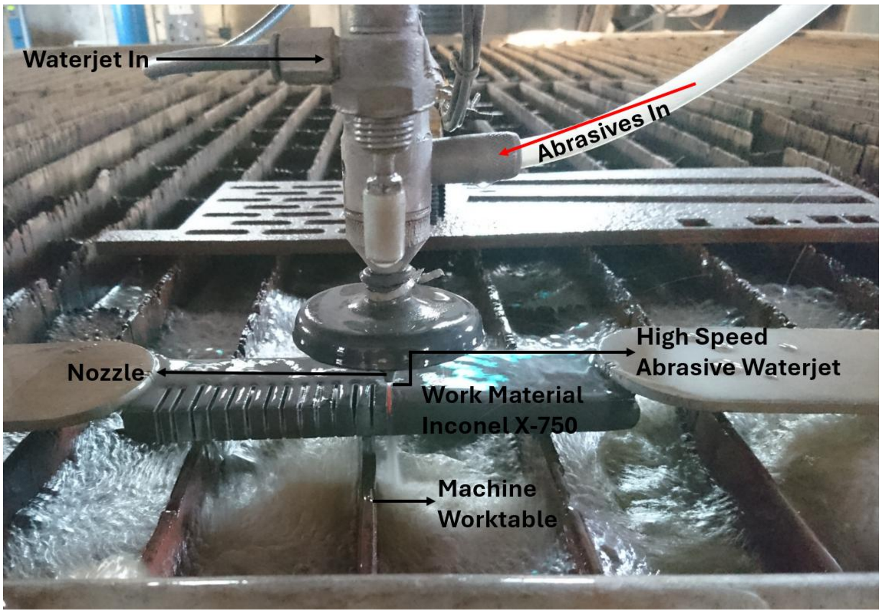

Figure 2. AWJM Experimental setup of the present work

The chemical composition of the work material, Inconel X-750 superalloy, was obtained hereby using the spectrographic analysis and is here tabulated in Table 1. The size of the work material is 200 × 50 × 15 mm. The properties of Inconel X-750 Superalloy are also tabulated in Table 2. In the AWJM, various abrasive materials can be used, like garnet, silica sand, aluminum oxide, olivine, glass beads, and zirconium. However, generally, garnet abrasives are used in industries due to their easy accessibility and low cost [21]. In this present study, the garnet is used as an abrasive particle with a mesh size #80 throughout the machining. Some physical attributes of garnet abrasives are given in Table 3. The appearance of garnet abrasives under the optical microscope is depicted in Figure 3.

Unlike any other process, the performance of the AWJM process is also influenced by different input parameters. These process parameters govern response characteristics (for example, surface roughness), which in turn decide the cut quality.

Table 1. Spectrographic analysis's resulting chemical composition of Inconel X-750 Superalloy

Element	Contents (%)
Nickel	Bal.
Chromium	15.50
Iron	7.00
Titanium	2.50
Aluminum	0.70
Niobium, Tantalum	1.00
Manganese	0.50
Copper	0.50
Silicon	0.20
Carbon	0.04
Cobalt	0.80

Table 2. Properties of Inconel X-750 Superalloy

Property	Unit	Value
Density	Kg/m^3	8280
Yield Strength	MPa	630
Ultimate Strength	MPa	1050
Hardness	RC	48.7
Elongation	%	19
Melting Temp. Range	°C	1393-1427
Curie Temperature	°C	48

Table 3. Properties of Garnet Abrasives [20-21], [34], [36]

Property	Values	Unit
Hardness	7	Moh Scale
Grit Size	Between 180 to 200	µm
Density	4100	kg/m^3
Shape	Sharp Edge Angular	---
Mesh Size	#80	---
Color	Red to Pink	---
Grade	Medium coarse	---

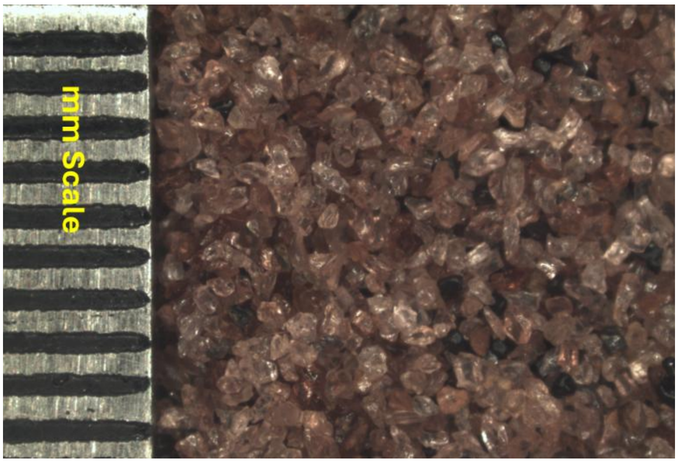

Figure 3. Appearance of garnet abrasives under optical microscopy

Therefore, within the present study, based on available machine setup, initial experiments and trail runs, and a critical review of available literature, three significant process parameters are explicit, which are the Water Pressure (WP), Standoff Distance (SOD), and Nozzle Traverse Speed (NTS) (sometimes regarded as traverse speed) which are finalized. Process parameter levels are also determined based on the previously available literature in the scientific domain, preliminary trial runs, and the variety of machine/experimental setups that are available. Table 4 displays the various process factor levels.

Table 4. Selected levels of process parameters

Parameters	Units	Level 1	Level 2	Level 3	Level 4	Level 4
SOD	mm	1	2	3	4	5
WP	MPa	320	340	360	380	400
TS	mm/min	20	30	40	50	60

The surface roughness tester (Make: Mitutoyo; Model: SJ-310), as depicted in Figure 4(a), is used to determine the Ra value of machined samples in the current experimental work. The R_a value is measured in three different regions of the samples, as shown in Figure 4(b): top region (the area of initial damage), the middle section (the area of smooth cutting), and the bottom region (the area of rough cutting). The R_a value is then averaged for additional analysis. The travel speed is 5 mm/second, with cut-off length λ_c= 0.8 mm with 5 divisions. So, the total traveling length found here is 4 mm.

Figure 4 (a). Surface roughness measurement device Mitutoyo SJ-310

Figure 4 (b). Sample highlighting the main region for R_a value measurement

A specialized vision measurement device (Make: Sipcon; Model: SDM-TRZ 5300) is used to measure the top and bottom region kerf widths of machined work material. To prevent the ballooning effect, the bottom kerf width is measured at a fixed height of 12 mm from the top surface. In Figure 5, this is illustrated. Eq. 1 is used to calculate the kerf taper further. The work material's top and bottom kerf widths following machining are shown in Figure 6.

$$\theta = tan^{-1}\left(\frac{W_t - W_b}{2t}\right) \tag{1}$$

where t is the thickness of the machined samples, W_t is the top width, W_b is the bottom width, and θ is the Kerf Taper angle.

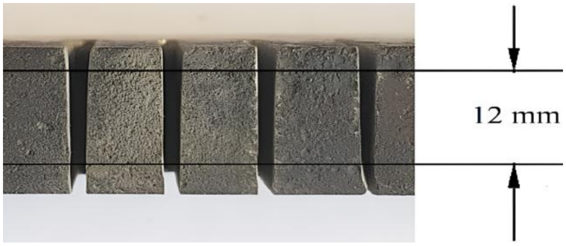

Figure 5: Kerf taper angle measurement

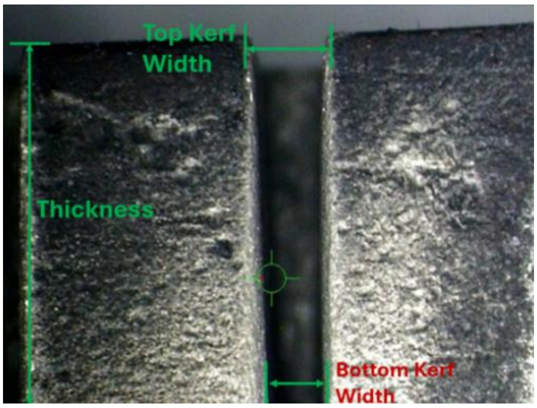

Figure 6. Top and bottom kerf width after machining operation representation

The MRR is a vital response characteristic in advanced machining processes. It is generally very low for advanced machining processes like EDM, ECM, EBM, etc. This represents the time taken to machine a certain amount of material. Therefore, to investigate the MRR in the case of the AWJM, a study was undertaken in the current study. The influence of the WP, TS, and SOD on the MRR of Inconel X-750 was used in abrasive waterjet machining. The MRR is measured in mm^3/min. It is the volume of material removed per unit of time. It is evaluated by using Eq. (2) [22 - 28]. The unit of MRR will be mm^3/min.

$$MRR = t \times W \times TS \tag{2}$$

where in Eq. (2), t is the thickness of workpiece material (in mm), also known as depth of penetration; W= Avg. Kerf Width ($W=W_t + W_b/2$), where W_t represents the Top Kerf width, W_b represents the Bottom Kerf width, and TS is the Traverse speed (mm/min).

3. RESULTS AND DISCUSSION

After the machining operation, the surfaces of the AWJM processed work material were carefully cleaned and examined. The cut surface was then taken for SR and kerf taper angle measurement. The results obtained were then analyzed. The Kerf top and bottom widths, traverse speed, penetration depth, and work material thickness were used to calculate the MRR. In Table 5, these response characteristics and process parameters are displayed.

Table 5. Process parameters and response characteristics for Inconel X-750

Exp. Runs Order as per CCD (RSM)	Process Parameters			Response Characteristics Obtained		
	X_A: WP (in MPa)	X_B: TS (in mm/min)	X_C: SOD (in mm)	R_a (in µm)	Kerf Taper Angle(θ) (degrees)	MRR (in mm^3/min)
1	340	30	2	4.561	0.67635	688.275
2	380	30	2	3.210	0.26403	695.000
3	340	50	2	5.954	1.19481	1060.000
4	380	50	2	5.035	0.78249	1202.630
5	340	30	4	5.999	0.88970	630.000
6	380	30	4	4.062	0.47741	686.250
7	340	50	4	6.917	1.40820	1045.500
8	380	50	4	6.532	0.99587	1158.380
9	320	40	3	6.305	1.24843	902.700
10	400	40	3	3.925	0.45300	1009.500
11	360	20	3	3.201	0.31765	460.000
12	360	60	3	7.115	1.36500	1300.000
13	360	40	1	4.652	0.64300	1007.700
14	360	40	5	6.077	1.08200	753.240
15	360	40	3	5.307	0.81500	860.000
16	360	40	3	5.282	0.78000	866.700
17	360	40	3	5.712	0.87900	854.700
18	360	40	3	5.684	0.79300	910.000
19	360	40	3	5.651	0.83611	890.000
20	360	40	3	5.622	0.80000	897.300

3.1 Surface Roughness (R_a)

Table 6 depicts the ANOVA table for R_a. The study and analysis are done with 95 percent confidence. The "F" Value of the model validates the importance of the fitted model. The most important factor affecting SR in the current investigation is the traverse speed. In general, the S/N ratio is measured by Adeq Precision, which is 27.699. A ratio greater than 4 is highly preferred, and it showed 27.699 ratios, which is a sufficient and essential signal. The design area can be navigated with the help of this model. With a difference of less than 0.2, the Predicted R^2 of 0.8904 and the Adjusted R^2 of 0.9196 were found here in satisfactory agreement.

Table 6. ANOVA for R_a

Source	Sum of Square	DOF	Mean Square	F-Value	P-Value	Remarks
Model	22.10	3	7.37	73.43	< 0.0001	Significant
X_A - WP	5.47	1	5.47	54.49	< 0.0001	
X_B - TS	13.02	1	13.02	129.81	< 0.0001	
X_C - SOD	3.61	1	3.61	35.99	< 0.0001	
Residual	1.60	16	0.1003			
Lack of Fit	1.41	11	0.1286	3.38	0.0946	Not Significant
Pure Error	0.1889	5	0.0389			
Cor Total	21.439	19				
Fit Statistics						
Std. Dev.	0.3167		R^2	0.9323		
Mean	5.34		Adj. R^2	0.9196		
C.V. %	5.93		Pred. R^2	0.8904		

Figure 7(a) shows how WP and TS affect the R_a of machined samples. The findings of the analysis show that the kinetic energy of the abrasive water jet automatically increases as the water pressure increases. It was found that the R_a decreased while the material was sliced smoothly along the machined surface. The extent of abrasive particles that impinge on the cutting surface is also reduced as the nozzle traverse speed increases. This reduces the cutting power of the jet, thereby increasing the surface roughness. The effects of water pressure and SOD on the surface roughness of machined samples are plotted in Figure 7(b). An increase in SOD causes jet flaring as the jet leaves the nozzle, lowering the jet's effective diameter. The reduced cutting capabilities of the jet resulted in an increase in surface roughness.

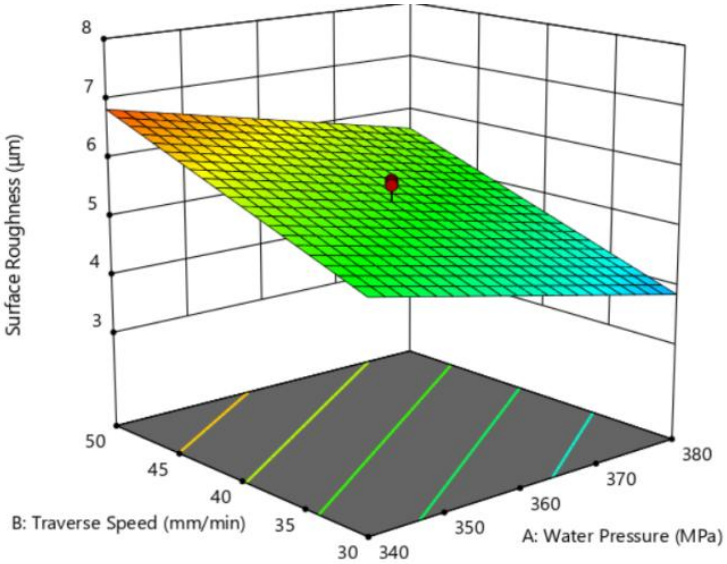

(a)

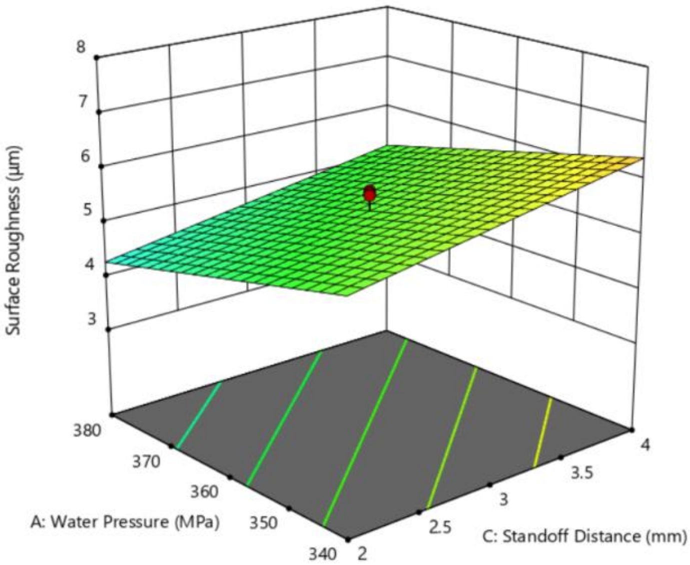

(b)

Figure 7. (a) Outcome of WP and Traverse Speed on R_a; (b) Outcome of WP and Standoff distance on R_a

3.2 Kerf Taper (θ)

Table 7 displays the Kerf Taper Angle ANOVA table. The study and analysis have a 95% confidence level. The "F" Value validates the significance of the fitted model. In this experiment, traversal speed is the most significant element influencing the kerf taper angle. The model is statistically significant with an F-value of 959.53, and the likelihood that undesirable random noise is the source of such a high F-value is 0.01%. In this analysis, several terms in the model are significant when the p-value is less than 0.05 [20-21]. Based on ANOVA, the significance of any parameter is determined using its p-value and F-value. The p-value determines the significance of any parameter. If the p-value is less than 0.05, the parameter is said to be significant. Further, the level of significance is determined by the F-value. The greater the F-value, the higher the significance will be, and vice versa. Consequently, it is determined that parameters X_A, X_B, and X_C are important contributors. On the other hand, p-values are greater than 0.1, indicating that a model term is statistically insignificant. Compared to the pure error, the lack of fit is not statistically significant, according to the Lack of Fit F-value of 0.30, with a 95.46% chance that the result could be the consequence of noise. This non-significant lack of fit indicates an excellent model fit with the experimental data. The model is reliable since the predicted R^2 value of 0.9928 and the Adjusted R^2 value of 0.9934 are nearly identical, with a difference of less than 0.2. The Adequate Precision value of 98.675 reflects a sufficient and high signal-to-noise ratio(S/N). This demonstrates that the model provides sufficient discrimination between meaningful signals and random variability, further validating its predictive capability. The design space can also be traversed using this model.

Table 7. ANOVA for Kerf Taper Angle

Source	Sum of Squares	DOF	Mean Square	F-Value	P-Value	Remarks
Model	1.93	3	0.6432	959.53	< 0.00010	significant
X_A-WP	0.6561	1	0.6561	978.85	< 0.00010	
X_B-TS	1.09	1	1.0900	1620.21	< 0.00010	
X_C-SOD	0.1874	1	0.1874	279.54	< 0.00010	
Residual	0.0107	16	0.0007			
Lack of Fit	0.0043	11	0.0004	0.3016	0.9546	not significant
Pure Error	0.0064	5	0.0013			
Corrected Total	1.94	19				
Fit Statistics						
Std. Dev.	0.0259		R^2	0.9945		
Mean	0.8351		Adj. R^2	0.9934		
C.V. %	3.10		Pred. R^2	0.9928		

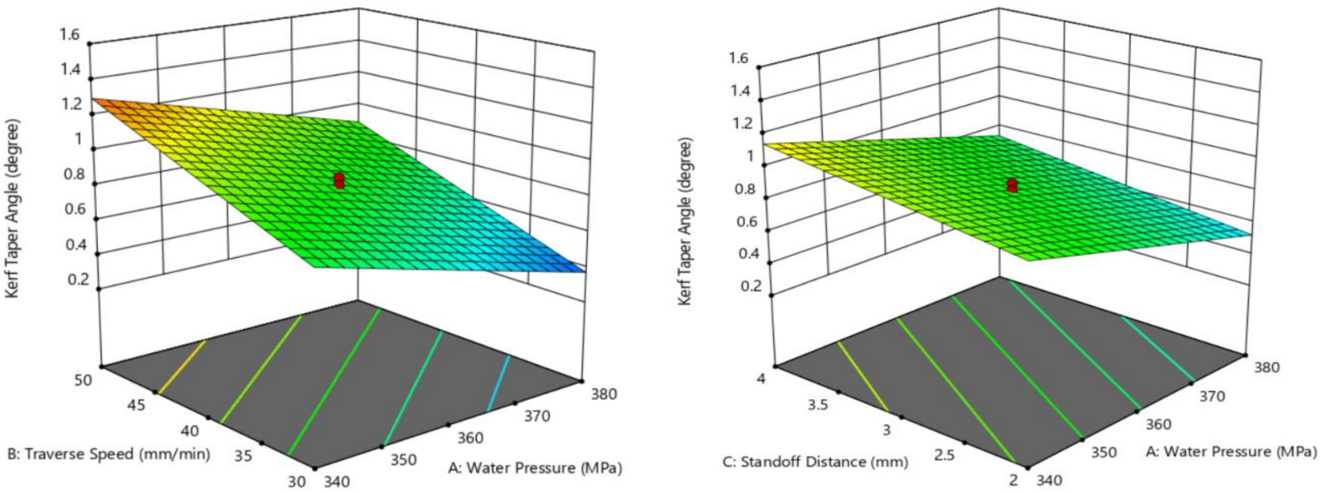

(a) (b)

Figure 8. (a) WP and TS Impact on Kerf Taper; (b) WP and SOD Impact on Kerf Taper

Figure 8(a) illustrates how the kerf taper angle of machined samples is affected by traverse speed and water pressure. An essential component of AWJM is the abrasive waterjet's kinetic energy. This kinetic energy rises with increasing water pressure. As the jet's cutting ability increases due to an increase in kinetic energy, the kerf taper lowers. Because fewer abrasives are impinging on the cutting surface, the jet's cutting effectiveness decreases as traverse speed increases. Consequently, the kerf taper increases. Figure 8(b) illustrates how SOD and water pressure affect the kerf taper of machined samples. Jet flaring rises with an increase in SOD. Jet flaring reduces the quantity of garnet abrasives in the jet's outer diameter. This causes the jet's effective diameter to decrease. Consequently, when the SOD rises, the kerf taper also rises as well.

3.3 The Rate of Material Removal

Table 8 displays the results of the MRR's ANOVA. With a 95% confidence level, the current study was conducted, and the model's validity was assessed using its F-value. With an F-value of 149.42, the model is statistically significant, indicating the likelihood that the enormous figure could be the consequence of undesirable random noise, which is a mere 0.01%. Furthermore, compared to the pure error, the Lack of Fit F-value of 4.61 indicates that the lack of fit is not statistically significant, suggesting that the model fits the data fairly well. A non-significant lack of fit demonstrates the reliability of the model. The adjusted R^2 value of 0.9591 and the predicted R^2 value of 0.9381 were found to be nearly identical, with a difference of less than 0.2, thus indicating here that the two values were consistent. A strong and dependable signal is indicated by the Adequate Precision score of 46.033, which gauges the S/N ratio, which is significantly higher than the suggested threshold of 4. The model's robustness and ability to precisely explore the design space mm^3/min are indicated by this high ratio.

Table 8. ANOVA Table for MRR

Source	Sum of Squares	DoF	Mean Square	F-value	p-value	
Model	7.855E+05	3	2.618E+05	149.42	< 0.0001	significant
X_A-WP	17693.99	1	17693.99	10.10	0.0058	
X_B-TS	7.426E+05	1	7.426E+05	423.81	< 0.0001	
X_C-SOD	25177.36	1	25177.36	14.37	0.0016	
Residual	28035.43	16	1752.21			
Lack of Fit	25519.44	11	2319.95	4.61	0.0521	not significant
Pure Error	2515.99	5	503.20			
Cor Total	8.135E+05	19				
Fit Statistics						
Std. Dev.	41.86		R^2	0.9655		
Mean	893.89		Adj. R^2	0.9591		
C.V. %	4.68		Pred. R^2	0.9381		

Figures 9(a) and (b), which exhibit the effects of WP and SOD on MRR, respectively, illustrate how WP and TP affect the MRR of machined samples. In considerable part, the traversal speed influences the MRR. The findings indicate that there is a direct correlation between it and the control variable. It is observed that when the traverse speed increases, the cutting rate improves, and more material is extracted from the target material in less time, resulting in an improvement in MRR. The high-energy water jet stream erodes the materials, resulting in material removal. At higher traverse speeds, more and more material is available for cutting, resulting in an increased MRR. It also increases due to the collective effect of TS and WP. It is due to the increased kinetic energy (KE) of the abrasive water jet. With such high KE, waterjet impacts the material, thereby eroding the material. In the current study, the influence of traverse speed is found to be very high, followed by WP and SOD. However, the statistical significance of traverse speed, along with the water pressure and standoff distance, is present in the present study. It is quite a possibility that due to the very high influence of the TS on MRR, the control of other process parameters is less registered on MRR. The results agree with the available literature [22 - 27]. Table 9 here shows the results obtained in the present study while compared with previous studies for MRR, surface, and kerf properties in the AWJM process for some specific superalloys.

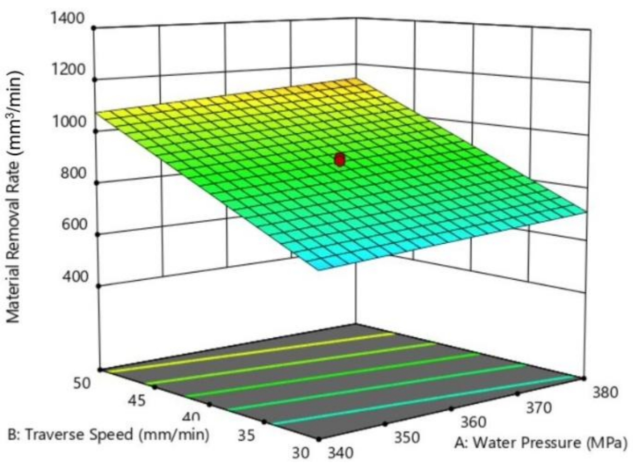

(a)

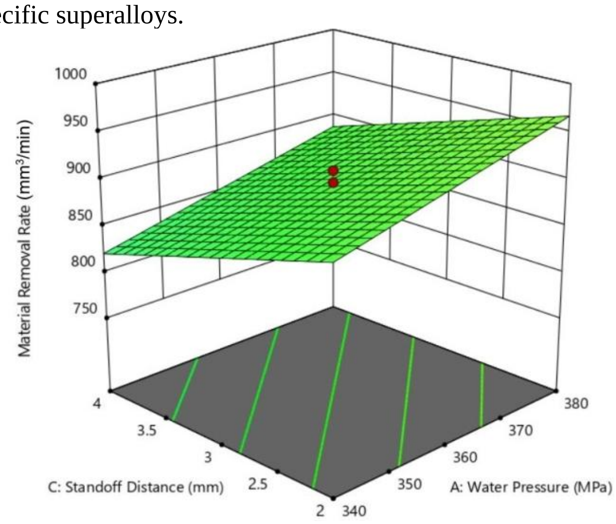

(b)

Figure 9. (a) WP and TS impact on MRR; (b) The impact of SOD and WP on MRR

Table 9. Results obtained in the present study are compared with previous studies for Material removal rate, surface roughness, and kerf properties in the AWJM process

Reference	Uthayakumar [33]	Reddy et al. [16]	Llanto [34]	Satyanarayana, and Srikar [8]	Saravanan et al., [35]	Present Study
Material	Inconel 600	Inconel-625	AISI 304 L	Inconel 718	Ti-6Al-4V alloy	Inconel X-750
Material Removal Rate	425 mm^3 /min	13.56 mm^3 /min	809.7 mm^3 /min	1053.2 mm^3 /min	48.81 mm^3 /min	907 mm^3 /min
Surface Roughness	4.129 μm	5.1 μm	1.9 μm	----	3.72 μm	4.1 μm
Kerf properties	----	0.72 mm (kerf width)	----	2.24 mm (kerf width)	----	0.4 degrees (kerf taper angle)

From Table 9, it is concluded that the results obtained in the present study are quite satisfactory compared to the literature. As reported by Uthayakumar [33], the MRR and surface roughness values are 425 mm^3/min and 4.129 µm. Further, as concluded by Reddy et al. [16], MRR, surface roughness, and kerf width values are 13.56 mm^3 /min, 5.1 µm, and 0.72 mm. As a result, obtained in the present study, the MRR, surface roughness, and kerf taper properties are 907 mm^3/min, 4.1 µm, and 0.4 degrees, which is quite a satisfactory outcome of the present research work.

4. REGRESSION MODEL DEVELOPMENT AND FITTING:

4.1 Regression Modelling for R_a:

The regression model was developed to predict SR (R_a) based on the most influential process parameters. The final model, expressed in coded factors (X_A, X_B, and X_C), is represented in Eq. (3). The response (R_a) can be predicted for particular values of each element using this coded equation, where high levels are represented by +1 and low levels by -1. It is advantageous to use the coded form in Eq. (3) to evaluate the relative importance of each parameter, as the factor’s coefficients show how strongly and in which direction each one influences the response. This approach facilitates a clearer understanding of how each factor contributes to the overall machining performance.

$$R_a = 5.34 - (0.5845 \times X_A) + (0.9021 \times X_B) + (0.475 \times X_C) \tag{3}$$

The predicted R² and adjusted R² values exhibit good agreement. This indicates that the model's predictions align well with the experimental data. This is also illustrated in Figure 10. The coefficients of the factors of Eq. (4) (represented in actual factors) provide insights into their relative significance by allowing direct comparison. Eq. (4) represents actual (non-coded) factors; hence, the factor levels must be supplied in their original measurement units when employing the equation stated in terms of those factors. This equation should not be utilized to ascertain the relative importance of various components, even though it may be useful for predictive analysis at specific factor levels. Because the intercept does not align with the center of the design space and the coefficients are scaled according to the units of each element, this may cause distortion in the impression of their individual impacts.

$$R_a = 10.83 - (0.0293 \times WP) + (0.0903 \times TS) + (0.475 \times SOD) \tag{4}$$

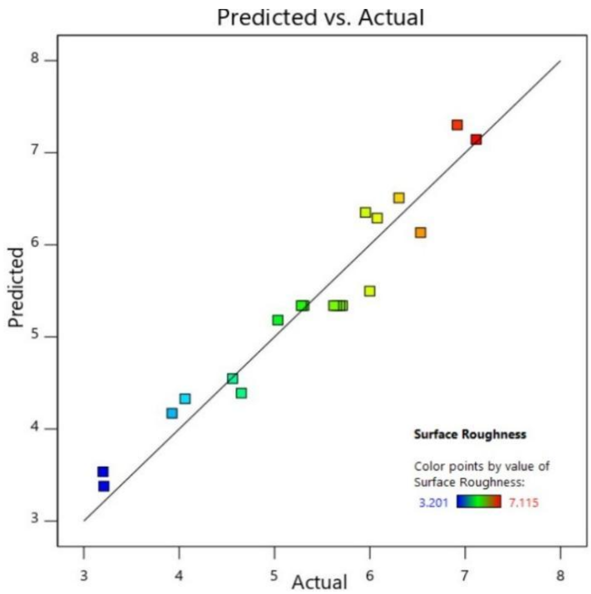

Figure 10. Predicted v/s actual plot for surface roughness

4.2 Regression Modelling for Kerf Taper

Regression models are created for important terms such as X_A, X_B, and X_C are coded factors, and the final regression model in terms of these factors is provided in Eq. (5).

$$Kerf\ Taper\ (\theta) = 0.835 - (0.2025 \times X_A) + (0.2605 \times X_B) + (0.1082 \times X_C) \tag{5}$$

The PredictedR^2value and AdjustedR^2value demonstrate a strong agreement. It shows that the expected outcome and the values measured experimentally agree. This is also illustrated in Figure 9. Additionally, the coefficients associated with the factors are instrumental in determining their relative significance by allowing for direct comparisons among them. Eq. (4) represents the predictive equation developed for the kerf taper angle in terms of actual components. The Predictive analysis of the reaction at predetermined values for each factor is made easier. It is necessary to express these levels in their original units. However, this equation should not be used to assess the relative relevance of each factor because these coefficients are scaled to represent the units of each parameter. Figure 11 displays the expected vs. actual for Kerf Taper.

$$Kerf\ Taper\ (\theta) = 3.114 - (0.011 \times WP) + (0.027 \times TS) + (0.109 \times SOD) \tag{6}$$

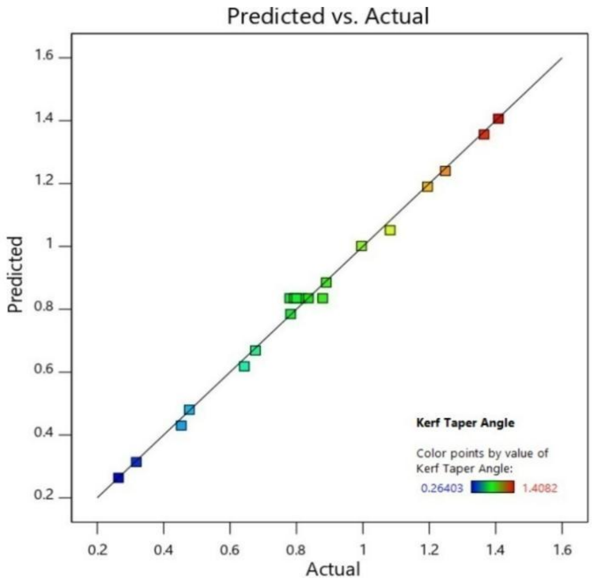

Figure 11. Predicted v/s Actual plot for Kerf Taper

4.3 Regression Modelling for Material Removal Rate

The reaction can be predicted at specific levels in the design space using Eq. (7), which is expressed as coded factors. Factors with higher levels are often coded as +1, whereas those with lower levels are coded as -1. Because it may be used to compare the factor coefficients and also to ascertain the relative impact of the components, the coded equation is very important. For specified levels of each element, the reaction can be predicted by using Eq. (8), which is expressed in real terms.

$$MRR = 893.89 + (33.25 \times X_A) + (215.44 \times X_B) - (39.67 \times X_C) \tag{7}$$

$$MRR = (-447.43) + (1.663 \times WP) + (21.544 \times TS) - (39.67 \times SOD) \tag{8}$$

The levels of each aspect in this situation ought to be expressed in their original units. The relative influence of each factor should not be determined using this equation since the intercept is not at the center of the design space, and the coefficients are scaled to fit the units of each element. Figure 12 compares the expected and actual rates of material removal. There is also a good agreement between the expected and actual values.

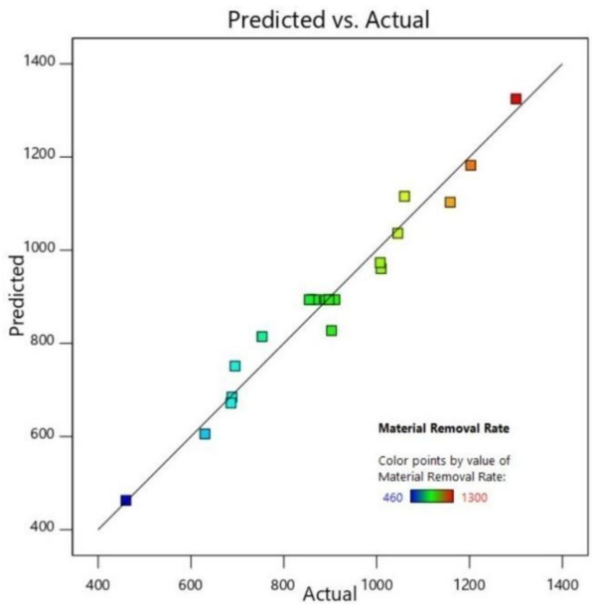

Figure12. Predicted v/s actual plot for material removal rate

4.4 Kerf Taper Properties, Material Removal Rate and Surface Roughness Optimization

The current work uses minimization-type criteria for process factor optimization with regard to both kerf taper and surface roughness. Regarding material removal rate, the optimization criterion is of the maximization type. The optimization problem becomes a minimization problem as both responses are being minimized. Table 10 shows the general criteria adopted for the optimization of process parameters in the present work.

Table 10. Criteria of optimization and optimum parameters for AWJM of Inconel X-750

Process Factor/ Process Response	Goal	Lower Limit (-1)	Upper Limit (+1)	Optimum Value post Optimization
WP (MPa)	Within Parameter Range	340	380	380
TS (mm/min)		30	50	38.6
SOD (mm)		2	4	2
Surface Roughness (R_a)	Minimization (↓)	3.31	7.115	4.1
Kerf Taper Angle (θ)		0.266	1.422	0.4
Material Removal Rate (MRR)	Maximization (↑)	460	1300	907

The optimized values of process parameters were taken, confirmation experiments were performed, and the responses were measured. Figure 13(a) represents the confirmation cuts made on Inconel X-750 post-optimization. Meanwhile, Figure 13(b) shows the optimized kerf taper obtained.

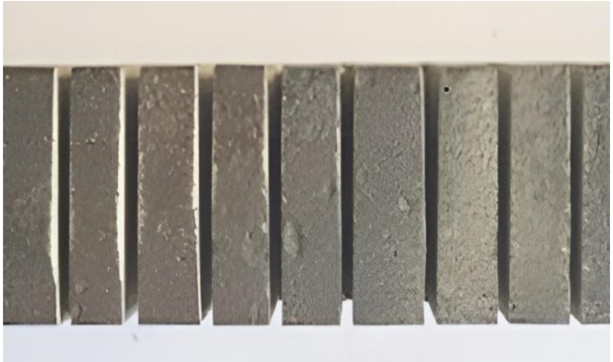

(a)

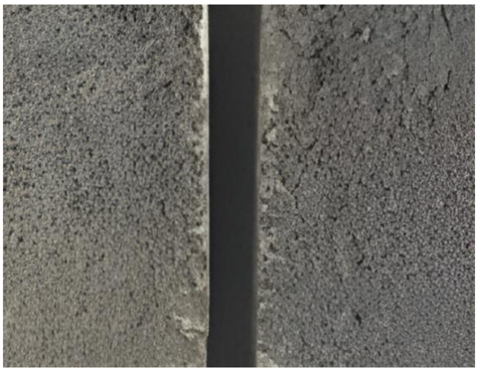

(b)

Figure 13. (a) Confirmations cuts made post optimization; (b) Optimized kerf taper characteristics of Inconel X-750

5. CONCLUSIONS

The current work is an experimental examination of how SR (R_a), kerf taper angle (θ), and MRR are affected by process parameters like WP, TS, and SOD. Inconel X-750 AWJM is carried out. The following results were found out in the current research work:

i) Based on ANOVA, the significance of each parameter on the performance characteristics of AWJM can be quantified. On this basis, the *p*-value of the most significant factor was found to be abrasive water jet pressure, traverse speed rate followed by SOD. The MRR, kerf taper properties and surface roughness could be improved by reducing the TS rate and SOD and increasing the water pressure (380 MPa).

ii) The water pressure (WP 380 MPa) increases, the MRR (907 mm^3/min) rises, whereas surface roughness (4.1 µm) and kerf taper angle (0.4°) decrease trends were noted.

iii) At high jet pressure, an abrasive water jet strikes work material with high kinetic energy at higher water pressure. This results in significant material removal. Due to higher kinetic energy, an abrasive water jet possesses higher momentum; upon striking the work material, there is momentum transfer. As the work material is held tightly on the machine table, the jet erodes and penetrates along the depth of the work material, creating a cut at a significantly larger level. This gives rise to a larger material removal rate of the work material. The benefit of higher MRR is that it reduces machining time and, ultimately, machining cost.

iv) The developed regression model can effectively predict the values of responses inside the design space and is well-fitted. The values measured experimentally and the model projections agree appropriately.

v) Additional process factor optimization is done to maximize MRR and reduce kerf taper and surface roughness. The optimized set process parameters post optimization was found to be WP of 380 MPa, TS of 38.6 mm/min, and SOD of 2 mm, which yielded surface roughness of 4.1 µm, kerf taper angle of 0.4 degrees, and MRR of 907 mm^3/min as optimized responses.

The work can be further extended by incorporating the influence of new process parameters, such as abrasive mass flow rate, different nozzle diameter, etc, on MRR, Surface roughness, and kerf taper angle. Further machine learning (ML) techniques can be implemented to model the pertaining problems of the presence of kerf taper angle and a lower surface finish. Further, the maximum possible penetrable depth without defect can be investigated as a scope of future work.

ACKNOWLEDGEMENT

Dr. Dharmalingam G would like to thank Vel Tech Rangarajan Dr. Sagunthala R&D Institute of Science and Technology for the financial support from RD fund, File No: VTU/RDF/FY 2023-2024/071.

CONFLICT OF INTEREST

The authors declare no conflicts of interest.

AUTHORS CONTRIBUTION

Vikas Sisodia (Conceptualization, Methodology, Validation; Data curation; Formal analysis; Visualization; Writing - original draft; Writing - review & editing)

Dharmalingam Ganesan (Methodology; Data curation; Validation; Resources, Software; Writing - review & editing),

Arun Prasad Murli (Methodology; Formal analysis; Visualization; Writing - review & editing)

Mithali Mane (Methodology; Formal analysis; Software; Visualization; Writing - review & editing)

Sachin Salunkhe (Conceptualization; Methodology; Formal analysis; Writing - review & editing; Project administration; Supervision)

Shailendra Kumar (Conceptualization; Methodology; Formal analysis; Writing - review & editing; Project administration; Supervision)

REFERENCES

[1] Geddes B, Leon H, Huang X, "Superalloys: alloying and performance," *ASM International*, 2010.

[2] W. J. Mills and L. A. James, "Effect of temperature on the fatigue-crack propagation behaviour of Inconel x-750," *Fatigue & Fracture of Engineering Materials & Structures*, vol. 3, no. 2, pp. 159–175, 1980.

[3] H. H. Jin, I. S. Ryu, S. Kim, J. Kwon, and G. G. Lee, "Contribution of microstructure to yield strength of X-750 alloy used for garter spring in Canada deuterium uranium reactor," *Journal of Nuclear Materials*, vol. 562, p. 153602, 2022.

[4] E. O. Ezugwu, J. Bonney, and Y. Yamane, "An overview of the machinability of aeroengine alloys," *Journal of Materials Processing Technology*, vol. 134, no. 2, pp. 233–253, 2003.

[5] T. Geethapriyan, R. M. Samson, A. C. A. Raj, S. Senkathi, and C. Gunasekar, "Parametric Optimization of Abrasive Water jet Machining Process on Inconel 600 Using Two Different Abrasive Grain Sizes," in K. Vijay Sekar, M. Gupta, A. Arockiarajan, (eds) *Advances in Manufacturing Processes, Lecture notes in Mechanical Engineering*, Springer Nature, pp. 457-469, 2018.

[6] Y. Natarajan, P. K. Murugesan, M. Mohan, and S. A. Liyakath Ali Khan, "Abrasive water jet machining process: A state of art of review," *Journal of Manufacturing Processes*, vol. 49, no. 49, pp. 271–322, 2020.

[7] D. S. Reddy, A. S. Kumar, and M. Sreenivasa. Rao, "Parametric optimization of abrasive water jet machining of inconel 800H using Taguchi methodology," *Universal Journal of Mechanical Engineering*, vol. 2, no. 5, pp. 158–162, 2014.

[8] B. Satyanarayana and G. Srikar, "Optimization of abrasive water jet machining process parameters using Taguchi Grey Relational Analysis (TGRA)," in *Proceedings of 13th IRF International Conference*, 20th July 2014, pp. 135-140.

[9] G. V. Kishore and F. Anand Raju, "Selection of optimum parameters for MRR & SR simultaneously in AWJM of Inconel-625 alloy using TOPSIS method, " *International Journal of Mechanical Engineering and Technology*, vol. 6, no. 9, pp. 1.9, 2015.

[10] G. Fowler, P. H. Shipway, and I. R. Pashby, "Abrasive water-jet controlled depth milling of Ti6Al4V alloy – an investigation of the role of jet–workpiece traverse speed and abrasive grit size on the characteristics of the milled material," *Journal of Materials Processing Technology*, vol. 161, no. 3, pp. 407–414, 2004.

[11] Y. I. Mogul, I. Nasir, and P. Myler, "Investigation and optimization for depth of cut and surface roughness for control depth milling in Titanium Ti6AL4V with abrasive water jet cutting," *Materials Today: Proceedings*, vol. 28, 2020, pp. 604–610.

[12] V. K. Pal and S. K. Choudhury, "Surface Characterization and Machining of Blind Pockets on Ti6Al4V by Abrasive Water Jet Machining," *Procedia Materials Science*, vol. 5, pp. 1584–1592, 2014.

[13] S. Vasanth, T. Muthuramalingam, P. Vinothkumar, T. Geethapriyan, and G. Murali, "Performance Analysis of Process Parameters on Machining Titanium (Ti-6Al-4V) Alloy Using Abrasive Water Jet Machining Process," *Procedia CIRP*, vol. 46, pp. 139–142, 2016.

[14] A. Alberdi, T. Artaza, A. Suárez, A. Rivero, and F. Girot, "An experimental study on abrasive waterjet cutting of CFRP/Ti6Al4V stacks for drilling operations," *The International Journal of Advanced Manufacturing Technology*, vol. 86, no. 1–4, pp. 691–704, 2015.

[15] Olsen, J. and Zeng, J. "The state-of-the-art of precision abrasive water jet cutting," in *Proceedings of the 8th Pacific Rim International Conference on Water Jet Technology*, p. 98032, 2006.

[16] P. Venkateshwar Reddy, G. Suresh Kumar, and V. Satish Kumar, "Multi-response optimization in machining inconel-625 by abrasive water jet machining process using WASPAS and MOORA," *Arabian Journal for Science and Engineering*, vol. 45, no. 11, pp. 9843–9857, 2020.

[17] B. Vasudevan, B. Vasudevan, L. Nagarajan, A. Karthick, C. Prakash, C. K. Chan, et al., "Experimental study, modeling, and parametric optimization on abrasive waterjet drilling of YSZ-coated Inconel 718 superalloy," *Journal of Materials Research and Technology*, vol. 29, pp. 4662–4675, 2024,

[18] P. Trivedi, A. Dhanawade, and S. Kumar, "An experimental investigation on cutting performance of abrasive water jet machining of austenite steel (AISI 316L)," *Advances in Materials and Processing Technologies*, vol. 1, no. 3–4, pp. 263–274, 2015.

[19] X. Wu, R. S. Chandel, H. Li, H. P. Seow, and S. Wu, "Induction brazing of Inconel 718 to Inconel X-750 using Ni–Cr–Si–B amorphous foil," vol. 104, no. 1–2, pp. 34–43, 2000.

[20] V. Sisodia, S. K. Gupta, S. Salunkhe, A. P. Murali, and S. Kumar, "An experimental investigation on machining of hardened AISI 440C stainless steel using abrasive water jet machining process," *Journal of Materials Engineering and Performance*, vol. 33, no. 2, pp. 961–977, 2023.

[21] S. Salunkhe, V. Sisodia, and J. P. Davim, *Abrasive Water Jet Machining of Composites: Empirical and Analytical Modelling*, vol. 21, Walter de Gruyter GmbH & Co KG, 2024.

[22] K. Ishfaq, N. A. Mufti, N. Ahmed, and S. Pervaiz, "Abrasive waterjet cutting of cladded material: kerf taper and MRR analysis," *Materials and Manufacturing Processes*, vol. 34, no. 5, pp. 544–553, 2018.

[23] J. M. Llanto, M. Tolouei-Rad, A. Vafadar, and M. Aamir, "Recent Progress Trend on Abrasive Waterjet Cutting of Metallic Materials: A Review," *Applied Sciences*, vol. 11, no. 8, p. 3344, 2021.

[24] I. Edriys, M. Fattouh, and R. Masoud, "Abrasive water jet machining of CFRPs: single response optimization using taguchi method optimization," *IOP Conference Series: Materials Science and Engineering*, vol. 973, p. 012029, 2020.

[25] A. Gnanavelbabu, P. Saravanan, K. Rajkumar, and S. Karthikeyan, "Experimental Investigations on Multiple Responses in Abrasive Waterjet Machining of Ti-6Al-4V Alloy," *Materials Today: Proceedings*, vol. 5, no. 5, pp. 13413–13421, 2018.

[26] S. Rammohan, S. T. Kumaran, M. Uthayakumar, K. Korniejenko, M. Nykiel, and A. Velayutham, "Prediction of abrasive waterjet machining parameters of military-grade armor steel by semi-empirical and regression models," *Materials*, vol. 15, no. 12, pp. 4368–4368, 2022.

[27] T. Manoharan, W. J. J. Thangaiah, S. Irulappasamy, and S. Dhar, "Study of delamination factors on the abrasive water-jet drilling of fibre metal laminates for military cargo aircraft," *Defence S and T Technical Bulletin*, vol. 11, pp. 248-59, 2018.

[28] G. Dharmalingam, S. Salunkhe, D. Panghal, A. P. Murali, S. Mahalingam, H. Tarigonda, et al., "Optimization of abrasive water jet machining process parameters on onyx composite followed by additive manufacturing," *Processes*, vol. 11, no. 8, pp. 2263–2263, 2023.

[29] Y. Qian, L. Wan, X. Wang, G. Zhang, X. Wang, and D. Li, "The cylindrical surface characteristics of AA7075 aluminum alloy machined by abrasive waterjet with circular cuts," *Journal of Materials Research and Technology*, vol. 26, pp. 4975–4988, 2023.

[30] A. C. Shekar, J.-P. Leclair, Redouane Zitoune, and L. A. Hof, "Surface engineering strategies for aerospace composite repairs: Machining and texturation of additive manufacturing parts by abrasive waterjet," *Wear*, pp. 205982–205982, 2025.

[31] Csaba Felhő, Krisztina Kun-Bodnár, and Z. Maros, "Comparison of 2D and 3D surface roughness parameters of AlMgSi0.5 aluminium alloy surfaces machined by abrasive waterjet," *Journal of Manufacturing and Materials Processing*, vol. 9, no. 3, pp. 80–80, 2025.

[32] N. E. Karkalos, M. Thangaraj, and P. Karmiris-Obratański, "Evaluation of the feasibility of the prediction of the surface morphologies of AWJ-Milled pockets by statistical methods based on multiple roughness indicators," *Surfaces*, vol. 7, no. 2, pp. 340-357, 2024.

[33] M. Uthayakumar, M. A. Khan, S. T. Kumaran, A. Slota, and J. Zajac, "Machinability of nickel-based superalloy by abrasive water jet machining," *Materials and Manufacturing Processes*, vol. 31, no. 13, pp. 1733–1739, 2015.

[34] M. Llanto, A. Vafadar, M. Aamir, and M. Tolouei-Rad, "Analysis and optimization of process parameters in abrasive waterjet contour cutting of AISI 304L," *Metals*, vol. 11, no. 9, p. 1362, 2021.

[35] M.P. Sudeshkumar, T. Maridurai, V. Suyamburajan, and V. Jayaseelan, "Optimization of SiC abrasive parameters on machining of Ti-6Al-4V alloy in AJM using Taguchi-Grey relational method," *Silicon*, vol. 14, no. 3, pp. 997-1004, 2021.

[36] T. M. Oh, G.-W. Joo, Y. Cha, and G.-C. Cho, "Effect of garnet characteristics on abrasive waterjet cutting of hard granite rock," *Advances in Civil Engineering*, vol. 2019, pp. 1–12, 2019.